Ultraclean layers and optically thin clouds in the stratocumulus to cumulus transition: Part II. Depletion of cloud droplets and cloud condensation nuclei through collision-coalescence

Kuan-Ting O*, Robert Wood and Christopher S. Bretherton

Department of Atmospheric Sciences, University of Washington, Seattle, Washington

Corresponding author address: Kuan-Ting O, Department of Atmospheric Sciences, University of Washington, Seattle, WA 98195.

E-mail: ktoandy@uw.edu

ABSTRACT

In part I, aircraft observations are used to show that ultraclean layers (UCLs) in the marine boundary layer (MBL) are a common feature of the stratocumulus to cumulus (Sc-Cu) transition region over the NE Pacific. The ultraclean layers are defined as layers of either cloud or clear air in which the concentration of particles with diameter larger than 0.1 μm is below 10 cm^{-3}. Here, idealized microphysical parcel modeling shows that in the cumulus regime, collision-coalescence can strongly deplete cloud droplet concentration in Cu updrafts thereby removing cloud condensation nuclei (CCN) from the atmosphere, suggesting that collision-scavenging is likely the key process causing the low particle concentration in UCLs. Furthermore, the model results suggest that the stratocumulus regime is typically not favorable for UCLs formation, because condensate amounts are generally not large enough to deplete drops in the time it takes to loft air to the upper PBL. A bulk parameterization of the coalescence-scavenging rate is derived based from in-situ measurements. The fractional coalescence-scavenging rate is found to be strongly dependent upon liquid water content (LWC), and hence the height above cloud base, indicating that higher cloud top and thus thicker cloud thickness in Cu updraft is an important factor accounting for the observed sharp rise of UCLs coverage in the Sc-Cu transition region. An important implication from this study is that planetary boundary layer (PBL) height, which controls maximum cloud thickness, and therefore LWC in updrafts, could be a crucial factor constraining efficiency of coalescence-scavenging and thus the formation of UCLs in MBL.

1. Introduction

The number concentration of water droplets N_d and cloud condensation nuclei (CCN) N_{ccn} continue to be variables of importance in marine boundary layer (MBL) clouds because they help determine cloud albedo (i.e., first indirect effect, Twomey 1977) and its perturbation due to aerosol can modulate the ability to form precipitation (Albrecht 1989). N_d is limited by N_{ccn} through the process of cloud droplet activation in which CCN serve as nuclei for cloud droplets. Changes in precipitation due to variations in N_d and N_{ccn} can enhance the change in cloud albedo associated with the Twomey effect. The smaller droplet size (i.e., smaller effective radius r_e) resulting from increasing N_d and N_{ccn} (for a given cloud liquid water content q_L) can hinder collision-coalescence and result in lower precipitation rate at cloud base R_{cb}, which could potentially increase cloud lifetime and hence cloud albedo, often called the second indirect effect (Albrecht 1989). Several observational studies have found a consistent relationship between R_{cb} and N_d in MBL clouds, and suggest that R_{cb} generally decreases as N_d increases (Hudson and Li 1995; Ferek et al. 2000; Bretherton et al. 2004; Wood 2005; Lu et al. 2007; Terai et al. 2012). However, there remain discrepancies in the degree of precipitation susceptibility to N_d and its dependence on liquid water path (LWP) and cloud thickness (H_t) across modeling and observational studies (Feingold and Siebert 2009; Sorooshian et al. 2009; Terai et al. 2015; Jung et al. 2016). Several studies have suggested that the changes in macrophysical processes such as entrainment rate in the MBL induced by aerosol perturbations can counter the second indirect effect and in some cases, may overcome it (Ackerman et al. 2004; Wood 2007; Bretherton et al. 2007; Small et al. 2009; Lee et al. 2012), emphasizing the difficulty in establishing a simple susceptibility metric.

Previous studies have focused upon variability of N_d and N_{ccn} as a driver of variability in precipitation. On the other hand, precipitation can also act as the driver of variability in N_d and

N_{ccn} through collision-coalescence. As pointed out by Hudson and Frisbie (1991), collision-coalescence can efficiently remove dissolved CCN within droplets from the atmosphere even with light precipitation rate (Feingold et al. 1996; Wood 2006). An evaporated coalesced droplet only leaves behind one residual haze particle that is made up of the nuclei from many droplets, the so-called coalescence-scavenging process, which is a irreversible process. Recently, by using a simplified aerosol budget model, driven by observations from aircraft and satellites, Wood et al. (2012) showed that the geographical and temporally variability of global MBL N_d and N_{ccn} are highly impacted by coalescence scavenging. This poses a potential positive feedback in the aerosol-cloud-precipitation interaction as suggested by recent modeling studies (Yang et al. 2012; Berner et al. 2013) such that the increase in N_{ccn} can reduce the efficiency of precipitation sink of N_{ccn}, which hence amplify the initial perturbation of increasing N_{ccn}.

In-situ measurements showing the coalescence-scavenging driving of the vertical variability in N_d and N_{ccn} have been presented in a mounting body of previous studies. Early in-situ measurements of marine cumulus have reported that there is a substantial decrease in N_d with increasing height (Weickmann and Aufm Kampe 1953; Squires 1958), suggesting the efficient depletion of N_d by collision-coalescence. Measurements of N_{ccn} in cumulus and stratocumulus decks over the northeastern Pacific Ocean (Hudson and Frisbie 1991; Hudson 1993) have shown there is definite vertical decrease of N_{ccn} which the authors attributed to coalescence-scavenging. Aircraft observations of MBL clouds over the southern Pacific ocean (Stephens and Platt 1987; Boers and Krummel 1998; Boers et al. 1996) have demonstrated that N_d generally decreases with increasing altitude while r_e shows the reverse trend, which is consistent with the occurrence of droplet growth by collision-coalescence. Similar vertical variations of N_d are also observed in midlatitude warm clouds and Arctic warm clouds as summarized by Gultepe and Isaac (2004). In recent observations over the southeastern Pacific Ocean, Terai et al. (2014) found that there is major vertical

stratification of N_{ccn} such that measurements at the surface can be a order of magnitude higher than those at the level of the main cloud deck within the pockets of open cells (POCs). For observations near the top of the PBL, N_d scaled strongly with vertical motion within active Cu (Wood et al. 2011). Further, N_d and N_{ccn} within POCs were found to be extremely low (~ 5 cm^{-3} in the mean), demonstrating that in-cloud collision-coalescence can be efficient in depleting N_d and N_{ccn}, especially in the upper MBL and prompting characterization of these layers as *ultraclean layers* (UCLs) (Sharon et al. 2006; Wood et al. 2011).

In Part I of this study (Wood et al. 2017), we demonstrated that during the Cloud System Evolution in the Trades (CSET) field program (CSET, Jul-Aug 2015, subtropical northeastern Pacific), the NSF/NCAR G-V aircraft frequently encountered UCLs, which were therein defined as layers of either cloud or clear air in which the concentration of of particles larger than 0.1 μm is below 10 cm^{-3} (see part I for details regarding the definition of UCLs). We showed that the clouds in the UCLs are typically geometrically thin and were commonly the veil clouds associated with aggregated Cu clusters. Visible satellite images indicate that a large fraction of clouds observed in the UCLs were optically thin ($\tau < 3$). In part, this is caused by the extremely low N_d in the UCL clouds (see discussion in part I). Aircraft in-situ measurements showed that (a) UCL coverage in CSET was as high as $40-60$ % between 135W and 155W (i.e., Sc-Cu transition region with deep planetary boundary layer height, hereafter PBL height) but that UCLs occurred very infrequently (< 10 %) east of 130W (i.e., the low-topped near-coastal stratocumulus region), (b) UCLs are mostly commonly found at a height of 1.5-2 km, typically close to top of the PBL and (c) r_e in the UCL clouds is ~ 20 μm in the mean, which is twice as large as the mean r_e in the non-UCL clouds (i.e., $N_d > 10$ cm^{-3}) (see Fig. 1).

Based on the analysis of the aircraft measurements summarized in Part I, we hypothesize that the observed UCLs most likely result from efficient collision-coalescence in the upper MBL over the

Sc-Cu transition region. The deep PBL height ($\sim 1500\,m$) in the Sc-Cu transition region gives high q_L in the active trade Cu towers. It provides an opportunity for collision-coalescence to sufficiently deplete N_d and hence could result in the formation of UCL clouds with extremely low N_d and large r_e in the upper MBL. Detrainment of cloudy air from the Cu towers forms horizontally extensive, thin cloud layers in the upper MBL with extremely low N_d and low cloud optical depth as indicated by the satellite data (see part I). Upon evaporation of UCL clouds, only a few accumulation mode particles are returned to the clear sky, which could leave the upper MBL strongly depleted in N_{ccn}.

In Part II of this work, we quantitatively test the proposed hypothesis for the formation process of the UCLs using idealized microphysical parcel model. The focus is on the depletion of N_d and N_{ccn} through in-cloud collision-coalescence. An adiabatic two-dimensional (i.e., spanning droplet and aerosol dry size) bin spectral parcel model is chosen as our main tool to test the hypothesis. The details of the model formulation are furnished in Sect. 2. Section 3 gives the parcel model results showing the temporal evolution of cloud microphysical processes in an idealized rising parcel in typical cumulus and stratocumulus regimes. In Sect. 4, by obtaining the best-fit with the in-situ measurements of cloud droplet size distributions (DSDs) from CSET, a bulk parameterization of the droplet coalescence-scavenging rate $[\dot{N}_d]_{cs}$ is derived from the stochastic collection equation as a function of N_d and q_L. With the parameterization, the relative importance of updraft, aerosol concentration, cloud thickness and adiabaticity in coalescence-scavenging process are accessed. Section 5 offers a conclusion.

2. Parcel model

a. Basic model formulations

A Lagrangian adiabatic parcel model with explicit two dimensional bin microphysics spanning aerosol and water droplet sizes is formulated to simulate the evolution of cloud microphysical processes in a rising parcel. First, the trajectory of the parcel follows an adiabatic ascent with a constant vertical velocity U_z. After the parcel reaches the assumed height of cloud top z_{top}, we include a period where the parcel moves horizontally as the cloud top layer with $U_z = 0$ (see Fig. 2). Cloud microphysical processes are considered by holding the particles on a two dimensional grid, and each grid point is characterized by the sizes of the dissolved aerosol and the water droplet. Grid spacing for the aerosol size (i.e., dry size) and the water droplet size (i.e., wet size) are logarithmically spaced. The grid of the droplet size starts and ends at D_d =0.02 μm and $D_d = 0.7$ cm. The aerosol size grid spans from D_a =0.016 μm to D_a =0.4 cm. Both liquid water and aerosol grids have 40 bins resulting in total 1600 bins in the 2-D grid space. The model is integrated with the time step of 0.05 s.

The prognostic thermodynamics variables are temperature and saturation ratio. The microphysical processes that are explicitly simulated in the model are activation of aerosol, condensation/evaporation, interstitial scavenging, collision-coalescence, and droplet loss from the parcel by sedimentation (the details regarding the treatments of droplet sedimentation process in the parcel model are given below). The details of the equations describing condensation and the changes of the thermodynamic variables applied in the model can be found in the appendix of Korolev and Mazin (2003). There is no artificial separation between unactivated aerosols, activated cloud droplets and drizzle. The nucleation of unactivated aerosol (i.e., haze particles) is explicitly calculated by solving the droplet growth equations. The κ-Kohler parameterization for aerosol hy-

145 groscopicity developed by Petters and Kreidenweis (2007) is applied and used to calculate the
146 saturation vapor pressure of all particles (the details regarding the size distribution and κ value of
147 aerosol are given later).

148 Collision-coalescence increases not only the size of water droplets but also size of the dissolved
149 aerosol inside. The advantage of the 2-D bin framework is that the resulting aerosol mass can be
150 saved after collision-coalescence takes place, which may be important for the temporal evolution
151 of DSDs. The hybrid bin scheme developed by Chen and Lamb (1994) (hereafter CL scheme)
152 is applied to treat condensation and evaporation processes. The two-dimensional flux method
153 developed by Bott (2000) (hereafter Bott scheme) is used to treat collision-coalescence in the 2-D
154 bin framework. Both the CL scheme and the Bott scheme are mass conservative and numerically
155 efficient. The CL scheme is a two-moment explicit scheme designed for the evolution of the DSDs
156 by condensation/evaporation, which produces little numerical diffusion and can be implemented
157 into the 2-D bin framework. The Bott scheme is an advanced method introducing the flux method
158 for the stochastic collection equations developed by Bott (1998) into the 2-D bin framework with
159 low artificial broadening of DSDs. The gravitational collection kernel is applied here and can be
160 given by $K(r,r') = E_c\pi(r+r')^2|V_T(r) - V_T(r')|$ (where E_c is the collision efficiency, r and r' are
161 the radius of droplets and V_T is the terminal velocity of droplet). The collision efficiency E_c used
162 in the collection kernel is based on the combination data from Hall (1980) and Rogers and Yau
163 (1989). The coalescence efficiency is set to unity. The inertial scavenging is considered in the
164 model with the collection kernel for inertial scavenging developed by Berner et al. (2013). It is
165 shown later that aerosol activation is the dominant process depleting N_{ccn}, and inertial scavenging
166 does not contribute significantly to the depletion of N_{ccn} in the cloud regime investigated here. The
167 terminal particle velocity V_T is based on the relationship of V_T with D_d given in Pruppacher and
168 Klett (2012).

b. Initial conditions and aerosol distribution

A set of initial conditions must be specified to run the model. The initial temperature T_0, the initial saturation ratio S_0 and the initial pressure P_0 are specified to be 300 K, 0.8, and 1013 hPa respectively, which are typical of the lower MBL and give the cloud base z_{base} (i.e., lifting condensation level, LCL) $\sim$ 500 m. The average normalized aerosol size distribution from the surface legs ($z < 170$ m) of 16 flights during CSET is used to specify the initial aerosol dry size spectrum in the model. The average aerosol size distribution shown in Fig. 3 is the combination of data from two probes, an ultra-high sensitivity aerosol spectrometer (UHSAS) ($0.06\ \mu m < D_a < 1\ \mu m$) and a cloud droplet probe (CDP) ($D_a > 1\ \mu m$). The CDP can quantify giant CCN (GCCN). The ambient size given by CDP is corrected to the dry size by using a 1.8 growth factor of sea salt as reported in Zhang et al. (2014). The sensitivity of the model results to GCCN is tested by removing GCCN from the initial aerosol input. The results (not shown) indicate that for the cloud regimes investigated here (i.e., in terms of number concentration of aerosol, aerosol size distribution, cloud top height and updraft speed), removal of GCCN from the initial aerosol input does not significantly change the temporal evolution of N_d and N_{ccn} in a rising parcel. GCCN could be relatively more important at the regime with more aerosol and lower cloud top height. To thoroughly explore the importance of GCCN for the droplet coalescence-scavenging rate, a more comprehensive study is needed to test the sensitivity to GCCN in various cloud regimes, which is not our focus in this study. Clarke et al. (2006) reported the mean aerosol size distribution over the coastal regions of Hawaii (i.e., the northeastern Pacific which is the same area investigated in this study) with average 10-m wind speed of $\sim$ 7 m s $^{-1}$. Note that the measurements in CSET only provide the aerosol size distribution with $D_a > 0.06\ \mu m$. To completely include the Aitken mode aerosol ($D_a < 0.1\ \mu m$), the aerosol concentration in size range $0.016\ \mu m < D_a < 0.06\ \mu m$

from Clarke et al. (2006) is included in the initial aerosol size distribution. The total initial aerosol concentration assigned in the parcel model will be discussed in Sect. 3. The κ value of aerosols is specified to be 0.8, which is typical at the surface over the northeastern Pacific according to a recent modeling study (see Figs. 3 and 5 in Pringle et al. 2010). When the initial aerosol size distribution is introduced into the 2-D aerosol and cloud bin spectrum, the initial equilibrium wet size of the aerosol is calculated based on the κ-Kohler equation with the specified κ value and the initial conditions of S_0, P_0 and T_0.

c. Treatment of droplet sedimentation in the parcel model

A significant deficiency of the Lagrangian parcel model is that droplet loss from the parcel by sedimentation is typically not taken into account. This may lead to unrealistic rates of collision-coalescence leading to the formation of millimeter-size drops with fall speeds substantially faster than the updrafts. This shortage in the Lagrangian approach can be avoided in Eulerian modeling frameworks like large eddy simulation (LES), which explicitly calculate droplet loss rate by sedimentation. On the other hand, in the Eulerian framework, the complexity of microphysical schemes is usually limited by computational resources, and cloud microphysical processes must typically be parameterized. With a focus in this study on microphysical processes for UCLs formation, we choose the 2-D bin microphysics parcel model as the tool for our modeling study. However, we also wish to consider the droplet loss due to sedimentation in the Lagrangian parcel model, and to achieve this, a simple treatment is selected and tested.

According to Houze (2014), with an assumption that the parcel has thickness h_p, the sedimentation loss rate of given size droplets in a parcel can be approximated by the sedimentation flux

$$[\dot{N_{i,j}}]_{sedi} = -N_{i,j}V_{T,j}/h_p \quad (1)$$

where i and j denote the aerosol dry size bin and droplet wet bin on the two-dimensional grid. A two step process is applied in the sedimentation flux method and is similar to the treatment in the 2-D collision-coalescence scheme proposed by Bott (2000). We first integrate the 2-D particle spectrum over the aerosol dry size which yields a 1-D droplet spectrum as a function of the droplet size. In the next step, the flux loss rate of droplet given in Eq. (1) is applied to each grid box of this intermediate spectrum. In the last step, the resulting new droplet spectrum is redistributed into the 2-D bin grids based on the fraction of droplets over the aerosol size grid before the sedimentation flux is applied. The parcel thickness h_p is specified to be 100 m and is also used to specify the depth of the cloud top layer (i.e., cloud top detrainment layer) in the simulation.

The most uncertain factor in the sedimentation flux method is h_p, which requires an assumption of the parcel thickness. The choices of h_p may make a significant difference in the results. It is shown later that there is only a weak sensitivity to h_p assumed in the model. In general, there is no perfect treatment for the droplet sedimentation process in the Lagrangian parcel model, so we will perform sensitivity tests to ensure our conclusion on the microphysical process of the UCLs is consistent among the parcel model runs with different assumed values of h_p.

3. Parcel modeling results

In part I, analysis of the aircraft measurements in CSET found that UCLs are commonly found between 135 W and 155W over the northeastern Pacific, the typical Sc-Cu transition region, but occur infrequently east of 130W over the northeastern Pacific, the overcast stratocumulus region. We showed that the UCL clouds are commonly the veil clouds associated with the aggregated Cu

clusters. This implies that the cumulus regime is favorable for the formation of UCLs. Here, two sets of idealized modeling representing the temporal evolution of cloud microphysics in a rising parcel in stratocumulus (hereafter Sc regime) and cumulus (hereafter Cu regime) are presented. According to Eastman et al. (2017), retrievals of PBL height from MODIS/CALIPSO and COSMIC GPS radio occulation show that the typical cloud-topped PBL heights at 20 N $\sim$ 40N are 1500 m between 135 W and 155W (i.e., Cu regime), and 800 m east of 130W (i.e., Sc regime) over the northeastern Pacific. These values are used to specify z_{top} in the parcel modeling for the Cu and Sc regimes, respectively. The updraft speeds U_z in MBL clouds are typically $0.1-3$ ms^{-1}, and U_z in cumulus is typically more vigorous than in stratocumulus (Comstock et al. 2007; Gerber et al. 2008; Ghate et al. 2011). Updraft velocity can influence both in-cloud times available for air parcels rising through a cloud and the maximum supersaturation ratio in a cloud updraft. The updraft speed U_z in the *base cases* for the Cu and Sc regimes are specified to be 0.75 ms^{-1} and 0.25 ms^{-1}, respectively. We will explore the sensitivity to updraft in both regimes by considering updraft velocities of 0.1 and 3 ms^{-1}. In the following discussion, N_d is defined as the number concentration of the particles with diameter ≥ 1 μm, and N_{ccn} is defined as the number concentration of the particles with diameter < 1 μm. The initial aerosol concentration with $D_a > 0.06$ μm is based on the mean near-surface (i.e., $z < 170$ m) aerosol concentration measured by the UHSAS probe (1 μm $> D_a > 0.06$ μm) during CSET (Fig. 4), and is specified to be 75 cm^{-3} (i.e., the mean value at 135W $\sim$ 155W, the typical cumulus regime) in the Cu regime, and 200 cm^{-3} (i.e., the mean value at 125W $\sim$ 132.5W, the typical stratocumulus regime) in the Sc regime. Note that the near-surface concentration of GCCN with $D_a > 1$ μm measured by CDP is mostly < 1 cm^3 in CSET. The aerosol concentration (~ 7 cm^{-3}) and size distribution with $D_a < 0.06$ μm from Clarke et al. (2006) is included in the initial aerosol distribution in both regimes to completely include the aitken mode aerosol. A summary of the input parameters applied in the Cu and Sc regimes is

given in Table 1. The discussion regarding liquid water content q_L in the parcel modeling will be given in Sect. 4.

a. Cumulus regime

Fig. 5 shows the base case for the Cu regime, which suggests the Cu regime is favorable for the formation of UCLs and supports our hypothesis. The modeling result shows that N_d is strongly depleted in the cumulus updraft, leading to the occurrence of UCL clouds at the cloud top layer. Surprisingly, there is substantial depletion (> 80 %) of N_d with height within the Cu updraft. Fig. 5-d shows the fraction of droplet loss caused by collision-coalescence, droplet sedimentation and evaporation. It indicates that collision-coalescence within the parcel is the dominant process in depleting N_d and the formation of UCLs in the Cu regime. The temporal evolution of r_e is shown in Fig 5-b with the black line, indicating considerable growth of droplet size in the Cu updraft by collision-coalescence. Cloud droplets can grow through condensation and collision-coalescence. By using an analytical expression for diffusional droplet growth, Pinsky et al. (2014) has shown that without including the collision-coalescence process, the r_e of droplets in warm liquid clouds can hardly reach 15 μm by condensation alone (see Fig. 6 in Pinsky et al. 2014). Thus, the substantial growth of r_e shown in the parcel modeling and the large r_e in UCL clouds observed during CSET (20 μm in the mean, see Fig. 1) must be due to collision-coalescence. The modeling results show that r_e can be larger than ~ 30 μm in the UCL clouds (black line in Fig. 5-b), and such large droplet size in the UCL clouds is also observed during CSET as shown in Fig. 1. After the parcel has reached its assumed max height, due to the relatively large droplet loss caused by droplet sedimentation (black line in Fig. 5-c), r_e in the UCL clouds decreases gradually. This may explain why the UCL cloudy samples observed during CSET have relatively large spread in r_e (see Fig. 1). After the parcel stops lifting, droplet sedimentation gradually becomes the

primary process depleting N_d (see Fig. 5-d) with very low droplet loss rate and very low droplet concentration (< 5 cm^{-3}). The results presented here suggest that there is a transition of dominant cloud microphysics process from the updraft to the cloud top layer such that the depletion of N_d is dominated by collision-coalescence resulting in the increase of r_e in the updraft, while at the cloud top layer, sedimentation loss is the main process depleting N_d and thus cause the decrease of r_e. Moderate Resolution Imaging Spectroradiometer (MODIS) retrievals of r_e suggests that such behavior of r_e is typical in the Sc-Cu transition region. Figure 6 shows that in the Cu clusters, r_e (from 3.7 micron MODIS channel) reduces from $\sim 30\ \mu m$ at the updraft region to $\sim 10\ \mu m$ at the cloud edge, which is consistent with the sedimentation process at the cloud top shown by the parcel modeling presented here. The schematic evolution of cloud microphysics in the cumulus updraft described here is summarized in Fig. 2.

The left panel in Fig. 7 shows the parcel modeling results for the Cu regime but with an artificially small U_z of 0.1 ms^{-1}. The cumulus case with U_z of 0.1 ms^{-1} has low S_{max} (~ 0.2 %) in the updraft, resulting in fewer particles activated at the cloud base than in the cases with U_z of 0.75 and 3 ms^{-1} (Fig. 5 and the right panels of Fig. 7). N_d in the Cu updraft is strongly depleted by collision-coalescence, which eventually cause the formation of UCLs in the updraft. In the case with low updraft of 0.1 ms^{-1}, UCLs is formed at fairly low altitude (~ 1100 m) even before the parcel reaches its assumed max height (i.e., 1500 m). Note that in the Cu cases with U_z of 0.75 and 3 ms^{-1}, UCLs are formed after the parcel reaches the assumed cloud top height. This indicates that slower U_z can help the formation of UCLs at lower altitude, which can be linked to the updraft time scale τ_{up} (i.e., a parcel to ascend from base to top) as discussed in Ovchinnikov et al. (2013). A longer τ_{up} (i.e., slower U_z, given same cloud thickness) can provide longer in-cloud time in updraft for collision-coalescence to act to deplete N_d, so the formation of UCLs is favored by slower updrafts (see detailed discussion in Ovchinnikov et al. (2013)). In addition to

the maximum supersaturation S_{max} at the cloud base, there is a second maximum in S_w occurring near the cloud top because of the substantial decrease of N_d (i.e., depletion term for supersaturation ratio S_w) and constant U_z in the Cu updraft (i.e., source term for S_w) (see equation 2 in Pinsky et al. 2013), leading to multiple secondary activation events of small aerosols (see Fig. 7-e) that can not be activated at the cloud base. Secondary activation of aerosols not only increases N_d but also hence slightly increases the droplet loss rate by collision-coalescence (droplet loss rate by collision-coalescence is positively correlated with N_d, see Eq. 3 in Sect. 4), which results in the blue jagged line of fraction of droplet loss by collision-coalescence shown in Fig. 7-d.

The right panel in Fig. 7 shows the parcel modeling result for the Cu regime with U_z of 3 ms^{-1}. Due to the high U_z (i.e., 3 ms^{-1}) assumed in this case, the available time for collision-coalescence to act to deplete N_d in the updraft is much shorter than in the other two cases (i.e., U_z= 0.1 and 0.75 ms^{-1}). The fractional loss of N_d from the cloud base to the cloud top $f_{top-loss}$ is $\sim$ 50 %, which is lower than in the case with U_z of 0.1 ms^{-1} and 0.75 ms^{-1} ($f_{top-loss} > 80$ %). Interestingly, in this case with high U_z, the maximum coalescence-scavenging rate (i.e., blue line in Fig. 7-h) is at the cloud top, while the maximum coalescence-scavenging rate in the previous cases with relatively lower updraft speed (i.e., Fig. 5 and left panel of Fig. 7) are typically not at the cloud top and their values are much lower (see blue lines in Figs. 5-c, 7-c and 7-h). This is because coalescence-scavenging rate is positively correlated with N_d and q_L (see Sect. 4 for details). In the cases with relatively low updraft (i.e., U_z= 0.1 and 0.75 ms^{-1}), most of N_d is depleted before the parcel reaches the cloud top. When the parcel reaches the cloud top, due to very low N_d ($<$ 10 cm^3), the coalescence-scavenging rate is very low, even though maximum q_L in the adiabatic updraft is at the cloud top. In contrast, in the case with fast U_z, more than 50 % of N_d still remain in the parcel at the cloud top where adiabatic q_L reaches its maximum in the updraft, resulting in the maximum coalescence-scavenging rate at the cloud top. Regarding the droplet size in the UCL

clouds, both of the modeling results shown in Fig. 7 suggest that r_e is $\sim 20\ \mu m$ in the UCL clouds, consistent with the observations shown in Fig. 1. The parcel modeling results for the Cu regime also suggest that UCL clouds contain a monomodal droplet size distribution, which is consistent with the observations summarized in Part I of this study. This indicates that the bin model can produce a droplet spectra in UCL clouds that is realistic compared with the observations. With the sensitivity test presented in Figs. 5 and 7 by considering a wide range of updraft speed in the Cu regime, we conclude that the parcel modeling results for the Cu regime agree well with the hypothesized microphysical process we proposed for UCL formation. The results indicate that in the Cu regime, collision-coalescence can cause the formation of UCL clouds by rapidly depleting N_d. Once the UCL clouds evaporate, this efficient coalescence-scavenging process can result in very low N_{ccn} in the upper MBL.

Fig. 8 shows a sensitivity test of the Cu base case to the choice of h_p applied in the sedimentation flux. The model runs with h_p of 100, 300 and 500 m are demonstrated here. The results shown in Fig. 8 all suggest that collision-coalescence is the key physical process controlling the depletion of N_d, and droplet loss by sedimentation is of secondary importance. The comparison between three model runs in Fig. 8 suggests that in the parcel, there is a compensating feedback in the parcel modeling between collision-coalescence and sedimentation processes in depleting N_d. When the parcel is assumed to be thinner (e.g., $h_p = 100$ m), large drizzle-sized droplets tend to fall out of the parcel faster by sedimentation (i.e., depleting N_d), but this lowers the efficiency of collision-coalescence by removing those drops that are the most efficient collectors, and vice versa. As a result of compensation between collision-coalescence and droplet sedimentation in the parcel model, the choice of h_p applied in the parcel model does not result in major differences in the temporal evolution of N_d. The parcel modeling runs for the Sc regime and the Cu regime with different U_z suggest the same compensating feedback (not shown). Thus, based on the sensitivity

test presented in Fig. 8, we conclude that the sedimentation treatment applied in the parcel model does not affect our conclusion that collision-coalescence is the process governing the formation of UCLs.

b. Stratocumulus regime

On the other hand, the modeling result of the Sc base case indicates that Sc regime is not favorable for the formation of UCLs (Fig. 9). One important feature in stratocumulus is that usually parcels would be forced to descend by long-wave cooling in a relatively short period of time than in cumulus. By using LES, Kogan (2006) showed that the residence time of air parcels at the cloud top is typically < 30 mins in stratocumulus. Thus, in the parcel modeling runs for the Sc regime, the time for which parcels stay in the cloud top layer is simply assumed to be 30 minutes. Although there is also an appreciable decrease of N_d caused largely by collision-coalescence, the fractional loss of N_d in the stratocumulus updraft is smaller than in the Cu updraft. N_d is 126 cm^{-3} when first reaching the cloud top, giving the fractional loss of 37.5 % from the cloud base (N_d is ~ 200 cm^{-3} at the cloud base). After the parcel stops lifting, there is a remarkable ripening effect (i.e., large droplets with positive growth rates continue to grow at the expense of small droplets with negative growth rates; see Celik and Marwitz 1999; Wood et al. 2002) which results in the evaporation of small droplets and thus an increase of $interstitial N_{ccn}$ (see Fig. 9-e) at the cloud top level. Droplet evaporation can contribute about 10 % of the droplet loss at the cloud top level in the Sc regime. On the contrary, in the Cu case, there is nearly no evaporation because droplets in the Cu updraft can grow to larger sizes (which have saturation vapor pressure ~ 100 %) due to higher S_{max} and more efficient collision-coalescence process in the Cu updrafts. At cloud top level in the Sc base case, when there is still a considerable concentration of droplets and aerosols, the droplet depletion rate by collision-coalescence becomes very low, preventing the formation of

UCLs at the cloud top layer. The mean r_e in the non-UCL clouds in the Sc base case is $\sim 10\ \mu m$, which is consistent with the in-situ measurements summarized in Fig. 1.

The left panel in Fig. 10 shows the modeling results for the Sc regime with U_z of 0.1 ms^{-1}. Due to low S_{max} caused by low U_z, a large fraction of aerosols are not activated at the cloud base. Due to long τ_{up} (because of low U_z) in the updraft and relatively small amount of activated aerosols compared with the Sc base case, UCL cloud ($N_d < 10\ cm^{-3}$) is formed at the cloud top layer mainly caused by collision-coalescence. This suggests that in the Sc regime, if U_z is low enough, formation of UCL cloud is possible, but due to low S_{max} and thus a large amount of unactivated aerosols remaining in the parcel, formation of a clear UCL (i.e., $N_{ccn} < 10\ cm^{-3}$) is difficult. Such low U_z ($\sim 0.1\ ms^{-1}$) in stratocumulus rarely occurs over the northeastern Pacific according to a recent observational study. Zheng et al. (2016) showed that observed cloud base updraft in stratocumulus over the northeastern Pacific are typically in the range of 0.2 - 1 ms^{-1}, which may explain why the observed occurrence of UCL clouds is fairly low ($< 10\ \%$) in the stratocumulus decks observed in CSET as we showed in Part I. The right panel in Fig. 10 shows the Sc case with U_z of 3 ms^{-1}, suggesting that high U_z in updraft can possibly result in nearly constant N_d vertical profile in stratocumulus, which is consistent with the previous discussion regarding fractional droplet loss and τ_{up} in the updraft. For both cases, r_e in the non-UCL clouds is $\sim 10\ \mu m$, consistent with the in-situ measurements shown in Fig. 1. Based on the parcel modeling results for the Sc regime shown in Figs. 9 and 10 with the sensitivity test on U_z, we conclude that the Sc regime is typically not favorable for UCL formation.

Although there are some major advantages to the adoption of a Lagrangian parcel model approach especially for the study focus on cloud microphysical processes, there are two major caveats should be addressed and discussed here: (1) the droplets falling into the parcel from above (2) the entrainment of aerosol from free troposphere are not taken into account, which could be the

significant source of droplet concentration in the rising parcel. However, the large droplet falling from above could also increase the efficiency of collision-coalescence by adding those drops that are the most efficient collectors, which can result in the compensating feedback as shown in Fig. 8. In addition, as shown in part I of this study, veil clouds in UCLs tend to be much less turbulent than non-UCL clouds in the same altitude, suggesting that the entrainment rate of aerosol from above into the veil clouds may be much lower than in the active cumulus updraft. Therefore, it seems very likely that these caveats would not affect our conclusion that UCLs should be the common feature throughout the trade cumulus regions of the subtropics further to the west of the Sc-Cu transitions, wherever the cumulus clusters typically precipitate with strong in-cloud collision-coalescence process.

4. Parameterization of droplet coalescence-scavenging rate

a. Derivation

The stochastic collection equation (SCE) gives an expression for the droplet loss rate through coalescence-scavenging $[\dot{N}_d]_{cs}$ (e.g., Wood (2006))

$$[\dot{N}_d]_{cs-SCE} = \frac{-1}{2}\int_0^\infty \int_0^\infty n(r)n(r')K(r,r')\,\mathrm{d}r\,\mathrm{d}r' \tag{2}$$

Given that each droplet coalescence event reduces the number of CCN by one, Eq. (2) can also be interpreted as being a loss rate for the CCN. To explicitly solve Eq. (2), a bin microphysics scheme and the full DSD is required. However, deployment of bin microphysics in a numerical model needs considerable computational expense, so the microphysical schemes in LES and general circulation model (GCMs) are mostly of the bulk form, which solve the prognostic equations only

for the bulk parameters such as N_d and q_L. Further, by using Eq. (2) and the parcel modeling, the time scale of droplet depletion and its dependence on N_d and q_L cannot be easily explored and examined. Thus, we use CSET observations to derive a parameterization for $[\dot{N}_d]_{cs-SCE}$ as a function of bulk parameters, which may provide more insight into the time scale of droplet depletion by collision-coalescence. In addition, with the parameterization of droplet coalescence-scavenging rate, we will explore the role of adiabaticity f_{ad} in the collision scavenging process. With the in-situ measurements of DSDs (i.e., droplet size distribution from CDP and 2DC probes of only the cloudy samples) from CSET (the details of the measurements used here and the criteria choosing the cloudy samples is summarized in Part I), we fit the following formula to the droplet loss rate calculated from the SCE (Eq. 2).

$$[\dot{N}_d]_{cs-PARAM} \; = \; -a(N_d)^b(q_L)^c \tag{3}$$

Note that units of $[\dot{N}_d]_{cs-PARAM}$, N_d and q_L in Eq. (3) are $[m^{-3}s^{-1}]$, $[m^{-3}]$ and $[kg\ m^{-3}]$. The values of a, b and c from the best-fitting are 8×10^4 (7×10^4, 9×10^4), 0.55 (0.545, 0.555) and 1.37 (1.36, 1.375). The values in the parentheses are the lower and upper confidence bounds with 95 % confidence level. Fig. 11 shows the comparison of Eq. (3) with the values calculated by SCE, indicating that the bulk parameterization of Eq. (3) agrees fairly well with the SCE (correlation coefficient = 0.84). It should be noted that most of the bulk microphysics models divide condensate into cloud and rain, and calculate the loss of N_d in terms of the sum of autoconversion and accretion processes. The derived droplet loss rate from SCE (Eq. 2) combine both of these effects, and describe them in terms of a single q_L, which is simpler then one would use in a bulk parameterization and is useful for our purpose here. To further examine the accuracy of the pa-

rameterization, $[\dot{N}_d]_{cs-BIN}$ calculated from the bin microphysics parcel model (i.e., blue lines in Figs. 5-c and 9-c) can serve as the benchmark for the parameterized formula of Eq. (3).

Figs 12-a and 12-d show the temporal evolution of N_d and q_L calculated from the parcel model in the Cu and Sc base cases (same as Figs. 5 and 9). Note that in Fig. 12, $q_L[parcel]$ is the liquid water content of the cloud droplets inside the parcel, and $q_L[parcel + sedimentation]$ is $q_L[parcel]$ plus the liquid water content lost to sedimentation. In both cases, the comparison of adiabatic q_L (calculated based on Eq. (19) from Pinsky et al. (2013)) with the output of q_L from the parcel model (i.e., $q_L[N_d + sedimentation]$) shows good agreement, indicating that the mass of the condensate is well conserved in the modeled adiabatic rising parcel. With the outputs of N_d and $q_L[N_d]$ from the parcel model, $[\dot{N}_d]_{cs-PARAM}$ can be calculated based on Eq. (3). Figs. 12-(b) and 12-(e) show the comparison of $[\dot{N}_d]_{cs-PARAM}$ with $[\dot{N}_d]_{cs-BIN}$ in the Cu and Sc base cases. The droplet loss rate calculated from the bin microphysics scheme and the parameterization are quite similar, suggesting that Eq. (3) could be a useful parameterization for $[\dot{N}_d]_{cs}$.

The maximum q_L in the Cu base case is three times as high as in the Sc base case because of the higher z_{top} assigned in the Cu base case. Interestingly, as the product of N_d and q_L, the values of $[\dot{N}_d]_{cs}$ are actually of the same order in two cases (N_d is higher in the Sc base case). Because the Cu and Sc base cases have different initial aerosol concentration assigned in the simulation, a better way to compare the efficiency of collision-coalescence is to use the fractional droplet loss rate given by

$$\frac{[\dot{N}_d]_{cs-PARAM}}{N_d} = -8 \times 10^4 (N_d)^{-0.45} (q_L)^{1.37} \tag{4}$$

Figs. 12-(c) and 12-(f) show the fractional loss rate of droplets in the Cu and Sc cases. The results indicate that the maximum fractional loss rate in the Sc base case is nearly five times smaller than in the Cu base case. In the Cu base case, the fractional loss rate can be higher than 20 % min^{-1}. On the contrary, the maximum fractional loss rate in the Sc base case is lower than 5 % min^{-1}. Given that the initial aerosol concentration in the Sc base case is twice as large as in the Cu base case, this further illustrates that the formation of UCLs is very unfavorable in the Sc regime.

With Eq. (4), the exponential time scale of droplet depletion by collision-coalescence can be written as

$$\tau_{cc}[s] = \frac{(N_d)^{0.45}(q_L)^{-1.37}}{8 \times 10^4} \tag{5}$$

Fig. 13 shows τ_{cc} calculated based on Eq. (5), indicating that the time scale of droplet depletion by collision-coalescence has strong dependence upon q_L but weak dependence upon N_d. This finding is consistent with the modeling results presented in Feingold et al. (1996), which suggests that the fractional droplet depletion rate by collision-coalescence is a strongly convex function of q_L and is almost independent of N_d (see Fig. 9 in Feingold et al. (1996)). Because q_L is proportional to the height above cloud base, it implies that the cloud thickness H_t is a more important factor constraining the coalescence-scavenging time scale in the MBL than is the aerosol concentration, as suggested in Wood (2006) (see Eq. (18) in Wood (2006)).

b. Fractional loss of droplets $f_{top-loss}$ and its dependence on U_z, N_d, H_t and f_{ad}

In this section, we derive a simple formula from Eq. (3) relating $f_{top-loss}$ with U_z, N_d, H_t and f_{ad} in order to access the relative importance of different factor in coalescence-scavenging process. By making an assumption that q_L increases linearly with the height z above cloud base, we can write

$$q_L = f_{ad}\Gamma_{ad}z \tag{6}$$

where Γ_{ad} is the adiabatic rate of increase of liquid water content with respect to height, and f_{ad} is the degree of adiabaticity with the range between 0 and 1. In stratocumulus, f_{ad} is often observed to be close to unity, particularly for nondrizzling stratocumulus (Albrecht et al. 1990; Zuidema et al. 2005). However, in cumulus, f_{ad} can be significantly lower because of entrainment and precipitation (Hobbs and Rangno 1996; Rauber et al. 2007). Several observational studies have shown that f_{ad} typically decreases with increasing altitude in cumulus (Hobbs and Rangno 1996; Rauber et al. 2007). Wood et al. (2009) showed that observed f_{ad} in cumulus can be parameterized by $z_0/(z_0+z)$, where z_0 is a scaling parameter, set to 500 m. Our main purpose here is to derive a simple formula relating $f_{top-loss}$ with U_z, N_d, H_t and f_{ad}, which is no longer possible if we retain the height dependence of f_{ad} in the derivation. Therefore, in this study, we assume f_{ad} is constant with height for simplicity. Γ_{ad} is assumed to have a fixed value of 2.1 $gm^{-3}km^{-1}$ which is typical for the MBL clouds in the subtropics and tropics (Albrecht et al. 1990). With Eq. (6), integrated liquid water path (LWP) from the cloud base to z can be written as

$$LWP(z) = \frac{f_{ad}\Gamma_{ad}z^2}{2} \tag{7}$$

By substituting q_L from Eq. (6) into Eq. (3) and dividing Eq. (3) by U_z, the decrease in N_d with increasing altitude can be given by

$$\frac{\mathrm{d}N_d}{\mathrm{d}z} = \frac{-a(N_d)^{0.55}(f_{ad}\Gamma_{ad}z)^{1.37}}{U_z} \tag{8}$$

The integration of Eq. (8) yields

$$\frac{(N_d)_z^{0.45} - (N_d)_{base}^{0.45}}{0.45} = \frac{-a(f_{ad}\Gamma_{ad})^{1.37} z^{2.37}}{2.37 U_z} \tag{9}$$

where $(N_d)_z$ is the number concentration of droplets at the altitude z, and $(N_d)_{base}$ is the number concentration of droplets activated at the cloud base. Then, by Eq. (9), the fractional loss of N_d from the cloud base to the cloud top $f_{top-loss}$ by collision-coalescence can be given by

$$\begin{aligned} f_{top-loss} &= 1 - \frac{(N_d)_{top}}{(N_d)_{base}} = 1 - (1 - \chi_{cc})^{2.2} \\ \chi_{cc} &= k \frac{(f_{ad})^{1.37} H_t^{2.37}}{(N_d)_{base}^{0.45} U_z} \\ k &= 0.19 a (\Gamma_{ad})^{1.37} \end{aligned} \tag{10}$$

where $(N_d)_{top}$ is the droplet concentration at the cloud top, and χ_{cc} is termed the *collision-coalescence efficiency factor*. The expression in Eq. (10) shows that $f_{top-loss}$ increases with the increase in f_{ad} and H_t, but decreases with the increase in U_z and $(N_d)_{base}$. The positive correlation of $f_{top-loss}$ with f_{ad} and H_t is straightforward. The droplet coalescence-scavenging rate is strongly dependent on q_L (see Section 4-a), so higher adiabaticity and deeper cloud depth (i.e., higher LWP) both increase the depletion of N_d through collision-coalescence. Regarding the negative correlation of $f_{top-loss}$ with U_z and $(N_d)_{base}$, the illustration is already given in Sect. 3 and Sect. 4-a. Fig. 14 shows contour plots of $f_{top-loss}$ against U_z, N_d, H_t and f_{ad} by assuming a reference U_z = 1 ms^{-1}, $(N_d)_{base}$ =75 cm^{-3}, H_t = 1000 m, and f_{ad} = 0.6. These values are used when they are not the variables in the contour plots (e.g., U_z = 1 ms^{-1} and f_{ad} = 0.6 are assumed in Fig. 13-a). To explore the sensitivity to the assumed reference values, another set of reference values is used

(i.e., U_z = 0.25 ms^{-1}, $(N_d)_{base}$ =200 cm^{-3}, H_t = 300 m, and f_{ad} = 1), and the results are shown in Fig. 15. The results calculated using two different sets of reference values are qualitatively very similar, which indicate that H_t is the most dominant factor determining $f_{top-loss}$, and $f_{top-loss}$ is found to be very insensitive to $(N_d)_{base}$. U_z is found to play more important role determining $f_{top-loss}$ than does f_{ad}. Overall, the relative importance of these factors determining $f_{top-loss}$ can be summarized as $H_t > U_z > f_{ad} > (N_d)_{base}$. This finding implies that H_t is a critical factor governing the efficiency of the coalescence-scavenging process.

5. Conclusions

In part I, based on the aircraft measurements from CSET, we found that ultraclean layers (UCLs) are common features in the Sc-Cu transition region over the northeastern subtropical Pacific ocean, and their fractional coverage can exceed $\sim$ 50 % where the PBL height exceeds 1 km. In part II of this study, the main goal is to test a hypothesis for the formation of UCLs in the MBL, namely that the deep PBL height over the Sc-Cu transition region can provide high q_L in the active Cu for collision-coalescence to sufficiently deplete N_d, resulting in low N_d and large r_e in clouds that are frequently observed in the upper MBL over the Sc-Cu transition region. Because of the efficient coalescence-scavenging process, after the evaporation of UCL clouds, only a few accumulation mode particles are returned to the clear sky, leaving very low N_{ccn} in the upper MBL.

A rising adiabatic parcel model with a 2D bin microphysics scheme is formulated to test the hypothesis. The results suggest that in the cumulus regime, collision-coalescence can efficiently deplete N_d, grow droplets, and remove N_{ccn} from the atmosphere in Cu updrafts, leading to the occurrence of UCLs in the upper MBL. In part I of this study, a case study with the geostationary satellite data has revealed that the UCL clouds are often associated with considerable amount of optically thin MBL clouds ($\tau < 3$). We postulate that the observed optically thin clouds are often

layers detraining from the active Cu towers in the upper MBL. The shallow depth and low N_d in these cloudy detrainment layers both contribute to the observed low cloud optical depth. The maintenance of these optically thin cloudy detrainment layers involves a balance between radiation, mesoscale ascent and cloud microphysics, which is certainly important but beyond the scope of our current paper. We leave that for a future LES study. On the other hand, the parcel modeling suggests that the formation of UCLs is typically not favored in the Sc regime. In summary, the idealized cloud parcel simulation in this work is able to explain the observed sharp rise of UCL coverage in the Sc-Cu transition region.

A parameterized expression for the droplet coalescence-scavenging rate $[\dot{N}_d]_{cs-PARAM}$ is derived as a function of bulk parameters N_d and q_L based on the in-situ measurements of DSDs from CSET. The comparison of $[\dot{N}_d]_{cs-PARAM}$ with the droplet loss rate derived from the SCE and the bin microphysics parcel model generally shows good agreement, suggesting that $[\dot{N}_d]_{cs-PARAM}$ is a useful parameterization. The derived parameters in $[\dot{N}_d]_{cs-PARAM}$ imply that the time scale of droplet depletion by collision-coalescence is strongly dependent upon q_L, but is weakly dependent upon N_d. An expression for the fractional droplet loss from the cloud base to the cloud top $f_{top-loss}$ by collision-coalescence is formulated as a function of a collision-coalescence efficiency factor χ_{cc} that depends on the cloud layer thickness, adiabaticity, updraft velocity, and cloud base droplet concentration. Of these factors, cloud thickness is the most dominant factor determining $f_{top-loss}$, and such finding is consistent with the results presented in Feingold et al. (1996) and Wood (2006). In the Sc-Cu transition region, the variation of cloud thickness is controlled mainly by cloud top height (i.e., cloud base heights do not vary as much as cloud top heights), which is constrained by PBL height. The implication is that PBL depth could play a crucial role governing the temporal and spatial variation of N_d and thus UCLs in the transition region, an issue that will be throughly explored in future work.

Acknowledgments. This research was supported by NSF Cloud System Evolution in the Trades (CSET) project (AGS-1445813). We thank Marcia Baker and Jørgen Jensen for helpful discussion.

References

Ackerman, A. S., M. P. Kirkpatrick, D. E. Stevens, and O. B. Toon, 2004: The impact of humidity above stratiform clouds on indirect aerosol climate forcing. *Nature*, **432 (7020)**, 1014.

Albrecht, B. A., 1989: Aerosols, cloud microphysics, and fractional cloudiness. *Science*, **245 (4923)**, 1227–1230, doi:10.1126/science.245.4923.1227.

Albrecht, B. A., C. W. Fairall, D. W. Thomson, A. B. White, J. B. Snider, and W. H. Schubert, 1990: Surface-based remote sensing of the observed and the adiabatic liquid water content of stratocumulus clouds. *Geophysical Research Letters*, **17 (1)**, 89–92.

Berner, A. H., C. Bretherton, R. Wood, and A. Muhlbauer, 2013: Marine boundary layer cloud regimes and poc formation in an les coupled to a bulk aerosol scheme. *Atmos. Chem. Phys*, **13 (12)**, 549–12.

Boers, R., J. B. Jensen, P. B. Krummel, and H. Gerber, 1996: Microphysical and short-wave radiative structure of wintertime stratocumulus clouds over the Southern Ocean. *Quarterly Journal of the Royal Meteorological Society*, **122 (534)**, 1307–1339, doi:10.1002/qj.49712253405, URL http://doi.wiley.com/10.1002/qj.49712253405.

Boers, R., and P. B. Krummel, 1998: Microphysical properties of boundary layer clouds over the Southern Ocean during ACE 1. *Journal of Geophysical Research*, **103 (D13)**, 16 651, doi:10.1029/97JD03280.

Bott, A., 1998: A flux method for the numerical solution of the stochastic collection equation. *Journal of the atmospheric sciences*, **55 (13)**, 2284–2293.

Bott, A., 2000: A flux method for the numerical solution of the stochastic collection equation: Extension to two-dimensional particle distributions. *Journal of the atmospheric sciences*, **57 (2)**, 284–294.

Bretherton, C., P. N. Blossey, and J. Uchida, 2007: Cloud droplet sedimentation, entrainment efficiency, and subtropical stratocumulus albedo. *Geophysical research letters*, **34 (3)**.

Bretherton, C. S., T. Uttal, C. W. Fairall, S. E. Yuter, and Coauthors, 2004: The epic 2001 stratocumulus study. *Bulletin of the American Meteorological Society*, **85 (7)**, 967.

Celik, F., and J. D. Marwitz, 1999: Droplet spectra broadening by ripening process. part i: Roles of curvature and salinity of cloud droplets. *Journal of the atmospheric sciences*, **56 (17)**, 3091–3105.

Chen, J.-P., and D. Lamb, 1994: Simulation of cloud microphysical and chemical processes using a multicomponent framework. part i: Description of the microphysical model. *Journal of the Atmospheric Sciences*, **51 (18)**, 2613–2630.

Clarke, A. D., S. R. Owens, and J. Zhou, 2006: An ultrafine sea-salt flux from breaking waves: Implications for cloud condensation nuclei in the remote marine atmosphere. *Journal of Geophysical Research: Atmospheres*, **111 (D6)**.

Comstock, K. K., S. E. Yuter, R. Wood, and C. S. Bretherton, 2007: The three-dimensional structure and kinematics of drizzling stratocumulus. *Monthly Weather Review*, **135 (11)**, 3767–3784.

Eastman, R., R. Wood, and K. T. O, 2017: The subtropical stratocumulus-topped planetary boundary layer: A climatology and the lagrangian evolution. *Journal of the Atmospheric Sciences*, **(2017)**.

Feingold, G., S. M. Kreidenweis, B. Stevens, and W. Cotton, 1996: Numerical simulations of stratocumulus processing of cloud condensation nuclei through collision-coalescence. *Journal of Geophysical Research-Atmospheres*, **101**, 21 391–21 402.

Feingold, G., and H. Siebert, 2009: Cloud-aerosol interactions from the micro to the cloud scale. perturbed clouds in the climate system: their relationship to energy balance, atmospheric dynamics, and precipitation. j. heintzenberg and r. charlson eds. MIT Press.

Ferek, R. J., and Coauthors, 2000: Drizzle suppression in ship tracks. *Journal of the Atmospheric Sciences*, **57 (16)**, 2707–2728.

Gerber, H., G. Frick, J. Jensen, and J. Hudson, 2008: Entrainment, mixing, and microphysics in trade-wind cumulus. *J. Met. Soc. Japan*, **86**, 87–106.

Ghate, V. P., M. A. Miller, and L. DiPretore, 2011: Vertical velocity structure of marine boundary layer trade wind cumulus clouds. *Journal of Geophysical Research: Atmospheres*, **116 (D16)**.

Gultepe, I., and G. a. Isaac, 2004: Aircraft observations of cloud droplet number concentration: Implications for climate studies. *Quarterly Journal of the Royal Meteorological Society*, **130 (602)**, 2377–2390, doi:10.1256/qj.03.120.

Hall, W. D., 1980: A detailed microphysical model within a two-dimensional dynamic framework: Model description and preliminary results. *Journal of the Atmospheric Sciences*, **37 (11)**, 2486–2507.

Hobbs, P. V., and A. L. Rangno, 1996: Precipitation from a maritime cloud layer with very low droplet concentrations. *Atmospheric Research*, **40 (1)**, 99–107, doi:10.1016/0169-8095(95)00030-5.

Houze, R. A., 2014: *Cloud dynamics*, Vol. 104. Academic press.

Hudson, J. G., 1993: Cloud condensation nuclei near marine cumulus. *Journal of Geophysical Research: Atmospheres*, **98 (D2)**, 2693–2702.

Hudson, J. G., and P. R. Frisbie, 1991: Cloud condensation nuclei near marine stratus. *Journal of Geophysical Research: Atmospheres*, **96 (D11)**, 20 795–20 808.

Hudson, J. G., and H. Li, 1995: Microphysical contrasts in atlantic stratus. *Journal of the atmospheric sciences*, **52 (16)**, 3031–3040.

Jung, E., B. A. Albrecht, A. Sorooshian, P. Zuidema, and H. H. Jonsson, 2016: Precipitation susceptibility in marine stratocumulus and shallow cumulus from airborne measurements. *Atmospheric Chemistry and Physics*, **16 (17)**, 11 395–11 413.

Kogan, Y. L., 2006: Large-eddy simulation of air parcels in stratocumulus clouds: Time scales and spatial variability. *Journal of the atmospheric sciences*, **63 (3)**, 952–967.

Korolev, A. V., and I. P. Mazin, 2003: Supersaturation of water vapor in clouds. *Journal of the atmospheric sciences*, **60 (24)**, 2957–2974.

Lee, S.-S., G. Feingold, and P. Y. Chuang, 2012: Effect of aerosol on cloud–environment interactions in trade cumulus. *Journal of the Atmospheric Sciences*, **69 (12)**, 3607–3632.

Lu, M.-L., W. C. Conant, H. H. Jonsson, V. Varutbangkul, R. C. Flagan, and J. H. Seinfeld, 2007: The marine stratus/stratocumulus experiment (mase): Aerosol-cloud relationships in marine stratocumulus. *Journal of Geophysical Research: Atmospheres*, **112 (D10)**.

Ovchinnikov, M., R. C. Easter, and W. I. Gustafson, 2013: Untangling dynamical and microphysical controls for the structure of stratocumulus. *Geophysical Research Letters*, **40 (16)**, 4432–4436.

Petters, M., and S. Kreidenweis, 2007: A single parameter representation of hygroscopic growth and cloud condensation nucleus activity. *Atmospheric Chemistry and Physics*, **7 (8)**, 1961–1971.

Pinsky, M., I. Mazin, A. Korolev, and A. Khain, 2013: Supersaturation and diffusional droplet growth in liquid clouds. *Journal of the Atmospheric Sciences*, **70 (9)**, 2778–2793.

Pinsky, M., I. Mazin, A. Korolev, and A. Khain, 2014: Supersaturation and diffusional droplet growth in liquid clouds: Polydisperse spectra. *Journal of Geophysical Research: Atmospheres*, **119 (22)**.

Pringle, K., H. Tost, A. Pozzer, U. Pöschl, and J. Lelieveld, 2010: Global distribution of the effective aerosol hygroscopicity parameter for ccn activation. *Atmospheric Chemistry and Physics*, **10 (12)**, 5241–5255.

Pruppacher, H. R., and J. D. Klett, 2012: *Microphysics of Clouds and Precipitation: Reprinted 1980*. Springer Science & Business Media.

Rauber, R. M., and Coauthors, 2007: Rain in shallow cumulus over the ocean: The rico campaign. *Bulletin of the American Meteorological Society*, **88 (12)**, 1912–1928.

Rogers, R. R., and M. Yau, 1989: A short course in cloud physics, international series in natural philosophy. Butterworth Heinemann, Burlington, MA.

Sharon, T. M., B. A. Albrecht, H. H. Jonsson, P. Minnis, M. M. Khaiyer, T. M. van Reken, J. Seinfeld, and R. Flagan, 2006: Aerosol and cloud microphysical characteristics of rifts and gradients in maritime stratocumulus clouds. *Journal of the atmospheric sciences*, **63 (3)**, 983–997.

Small, J. D., P. Y. Chuang, G. Feingold, and H. Jiang, 2009: Can aerosol decrease cloud lifetime? *Geophysical Research Letters*, **36 (16)**.

Sorooshian, A., G. Feingold, M. D. Lebsock, H. Jiang, and G. L. Stephens, 2009: On the precipitation susceptibility of clouds to aerosol perturbations. *Geophysical Research Letters*, **36 (13)**.

Squires, P., 1958: The spatial variation of liquid water and droplet concentration in cumuli. *Tellus A*, **10 (3)**.

Stephens, G. L., and C. M. R. Platt, 1987: Aircraft Observations of the Radiative and Microphysical Properties of Stratocumulus and Cumulus Cloud Fields. *Journal of Applied Meteorology*, **26 (9)**, 1243–1269, doi:10.1175/1520-0450(1987)026⟨1243:AOOTRA⟩2.0.CO;2.

Terai, C., R. Wood, and T. Kubar, 2015: Satellite estimates of precipitation susceptibility in low-level marine stratiform clouds. *Journal of Geophysical Research: Atmospheres*, **120 (17)**, 8878–8889.

Terai, C., R. Wood, D. Leon, and P. Zuidema, 2012: Does precipitation susceptibility vary with increasing cloud thickness in marine stratocumulus? *Atmospheric Chemistry and Physics*, **12 (10)**, 4567–4583.

Terai, C. R., C. S. Bretherton, R. Wood, and G. Painter, 2014: Aircraft observations of aerosol, cloud, precipitation, and boundary layer properties in pockets of open cells over the southeast Pacific. *Atmospheric Chemistry and Physics*, **14 (15)**, 8071–8088, doi:10.5194/acp-14-8071-2014.

Twomey, S., 1977: The Influence of Pollution on the Shortwave Albedo of Clouds. *Journal of the Atmospheric Sciences*, **34 (7)**, 1149–1152, doi:10.1175/1520-0469(1977)034⟨1149:TIOPOT⟩2.0.CO;2.

Weickmann, H., and H. Aufm Kampe, 1953: Physical properties of cumulus clouds. *Journal of Meteorology*, **10 (3)**, 204–211.

Wood, O., Robert, and Coauthors, 2017: Ultraclean layers and optically thin clouds in the stratocumulus to cumulus transition: Part i. observations. *Journal of the atmospheric sciences*, submitted.

Wood, R., 2005: Drizzle in Stratiform Boundary Layer Clouds. Part II: Microphysical Aspects. *Journal of the Atmospheric Sciences*, **62 (9)**, 3034–3050, doi:10.1175/JAS3530.1.

Wood, R., 2006: Rate of loss of cloud droplets by coalescence in warm clouds. *Journal of Geophysical Research: Atmospheres*, **111 (D21)**.

Wood, R., 2007: Cancellation of aerosol indirect effects in marine stratocumulus through cloud thinning. *Journal of the atmospheric sciences*, **64 (7)**, 2657–2669.

Wood, R., C. Bretherton, D. Leon, A. Clarke, P. Zuidema, G. Allen, and H. Coe, 2011: An aircraft case study of the spatial transition from closed to open mesoscale cellular convection over the southeast pacific. *Atmos. Chem. Phys*, **11 (5)**, 2341–2370.

Wood, R., S. Irons, and P. Jonas, 2002: How important is the spectral ripening effect in stratiform boundary layer clouds? studies using simple trajectory analysis. *Journal of the atmospheric sciences*, **59 (18)**, 2681–2693.

Wood, R., T. L. Kubar, and D. L. Hartmann, 2009: Understanding the importance of microphysics and macrophysics for warm rain in marine low clouds. part ii: Heuristic models of rain formation. *Journal of the Atmospheric Sciences*, **66 (10)**, 2973–2990.

Wood, R., D. Leon, M. Lebsock, J. Snider, and A. D. Clarke, 2012: Precipitation driving of droplet concentration variability in marine low clouds. *Journal of Geophysical Research: Atmospheres*, **117 (D19)**.

Yang, Q., and Coauthors, 2012: Impact of natural and anthropogenic aerosols on stratocumulus and precipitation in the southeast pacific: a regional modelling study using wrf-chem. *Atmospheric Chemistry and Physics*, **12 (18)**, 8777–8796.

Zhang, X., P. Massoli, P. K. Quinn, T. S. Bates, and C. D. Cappa, 2014: Hygroscopic growth of submicron and supermicron aerosols in the marine boundary layer. *Journal of Geophysical Research: Atmospheres*, **119 (13)**, 8384–8399.

Zheng, Y., D. Rosenfeld, and Z. Li, 2016: Quantifying cloud base updraft speeds of marine stratocumulus from cloud top radiative cooling. *Geophysical Research Letters*, **43 (21)**.

Zuidema, P., E. R. Westwater, C. Fairall, and D. Hazen, 2005: Ship-based liquid water path estimates in marine stratocumulus. *Journal of Geophysical Research: Atmospheres*, **110 (D20)**.

LIST OF TABLES

718 TABLE 1. Input parameters for the Cu and Sc regimes applied in the parcel model. Initial N_{ccn} includes both
719 aitken mode and accumulation mode aerosol measured during CSET and from Clarke et al. (2006). See Sect. 2
720 and Sect. 3 for details.

Input parameters	*Cumulus*	*Stratocumulus*
Initial N_{ccn} $[cm^{-3}]$	77	207
z_{top} $[m]$	1500	800

LIST OF FIGURES

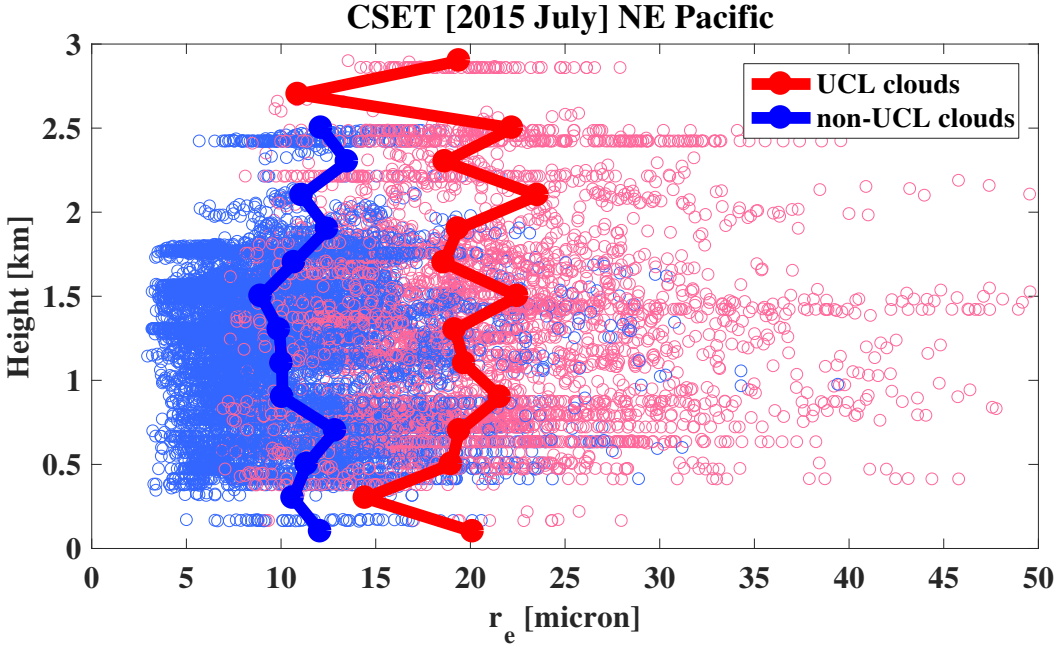

FIG. 1. Cloud droplet effective radius r_e of UCL clouds (red) and non-UCL clouds (blue) measured during CSET. The blue and red lines are the mean r_e of non-UCL clouds and UCL clouds. The calculation of r_e is based on the measured DSDs of the CDP and 2DC probes. UCL cloud is defined as the cloudy layer with $N_d < 10\ cm^{-3}$, and non-UCL cloud is defined as the cloudy layer with $N_d > 10\ cm^{-3}$. The criterion used to separate the saturated cloudy samples from the unsaturated clear-air samples can be found in part I of this study.

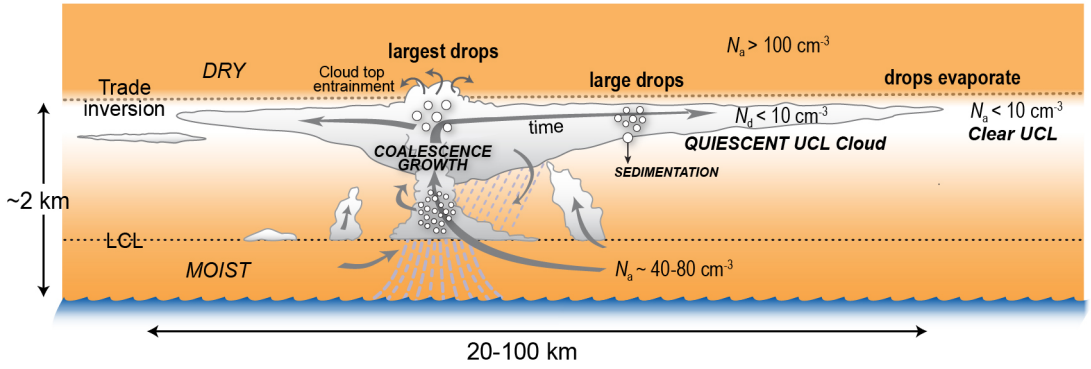

FIG. 2. Conceptual diagram of the formation of ultraclean layers in the Sc-Cu transition.

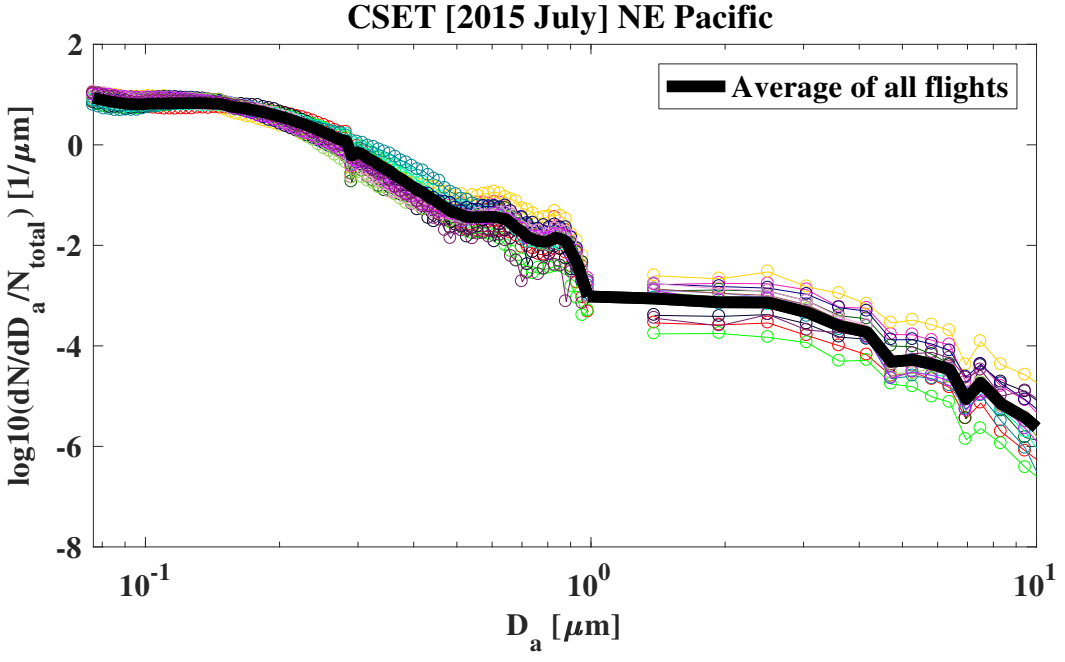

779 FIG. 3. Average normalized aerosol size distribution from CSET surface legs ($z < 170\ m$) of 16 flights
780 (colors, with circle) based on the UHSAS and CDP probes. The black line is the average normalized aerosol
781 size distribution from all flights.

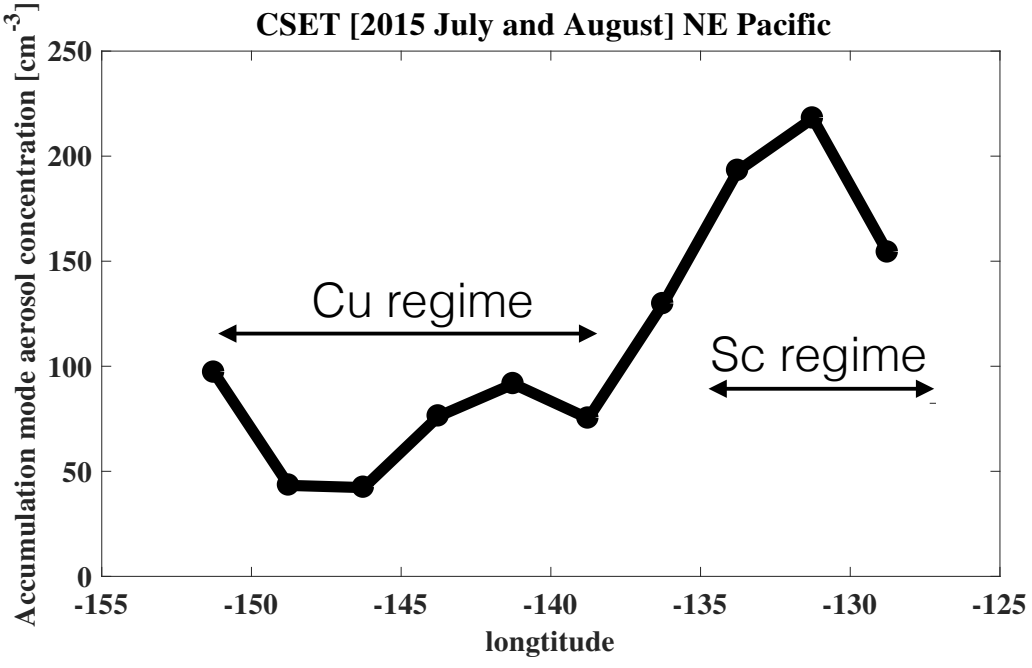

782 FIG. 4. Average accumulation mode aerosol concentration from CSET surface legs ($z < 170\ m$) as a function
783 of longitude based on the UHSAS probe.

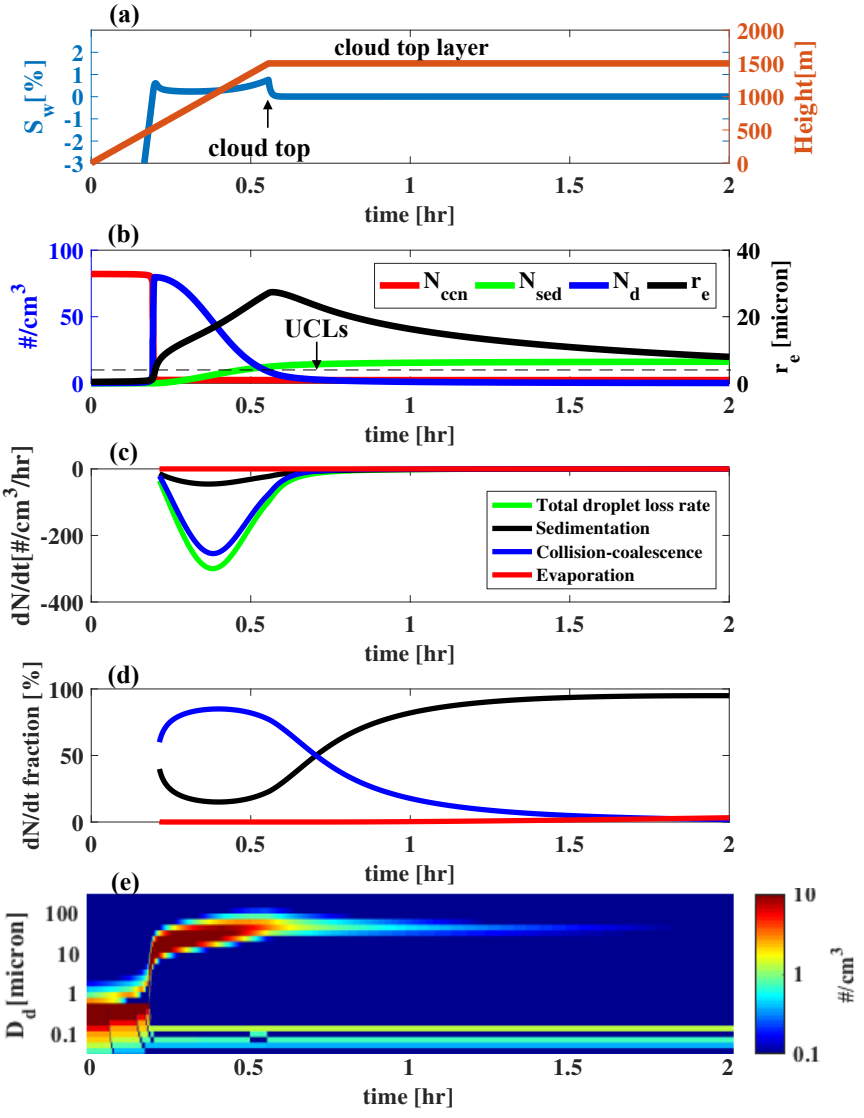

784 FIG. 5. Cumulus base case with U_z of 0.75 ms^{-1}. (a) Height (orange) and supersaturation ratio (blue) of
785 the parcel; (b) Temporal evolution of number concentration of cloud condensation nuclei N_{ccn} (red), droplet
786 sedimentation N_{sed} (green), cloud droplet N_d (blue) and effective radius of droplet r_e (black) in the parcel,
787 and the black dotted lines indicates particle concentration $= 10\ cm^{-3}$; (c) Total droplet loss rate (green) and
788 the droplet loss rate by sedimentation (black), collision-coalescence (blue) and evaporation (red); (d) Fraction
789 of droplet loss rate by sedimentation (black), collision-coalescence (blue) and evaporation (red); (e) Temporal
790 evolution of DSDs in the parcel.

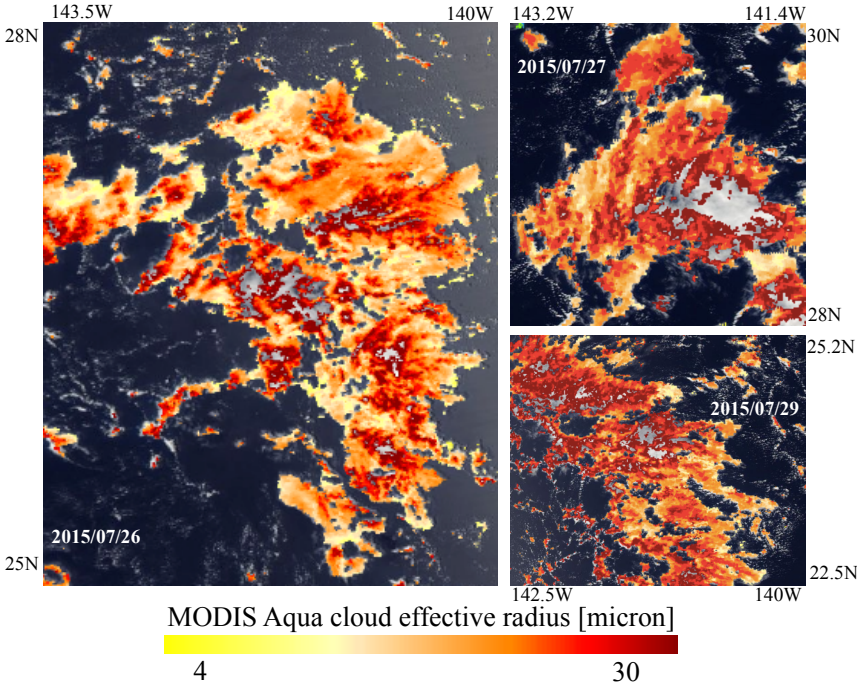

FIG. 6. MODIS retrieval of effective radius of Cu clusters in the Sc-Cu transition [3.7 micron MODIS channel]

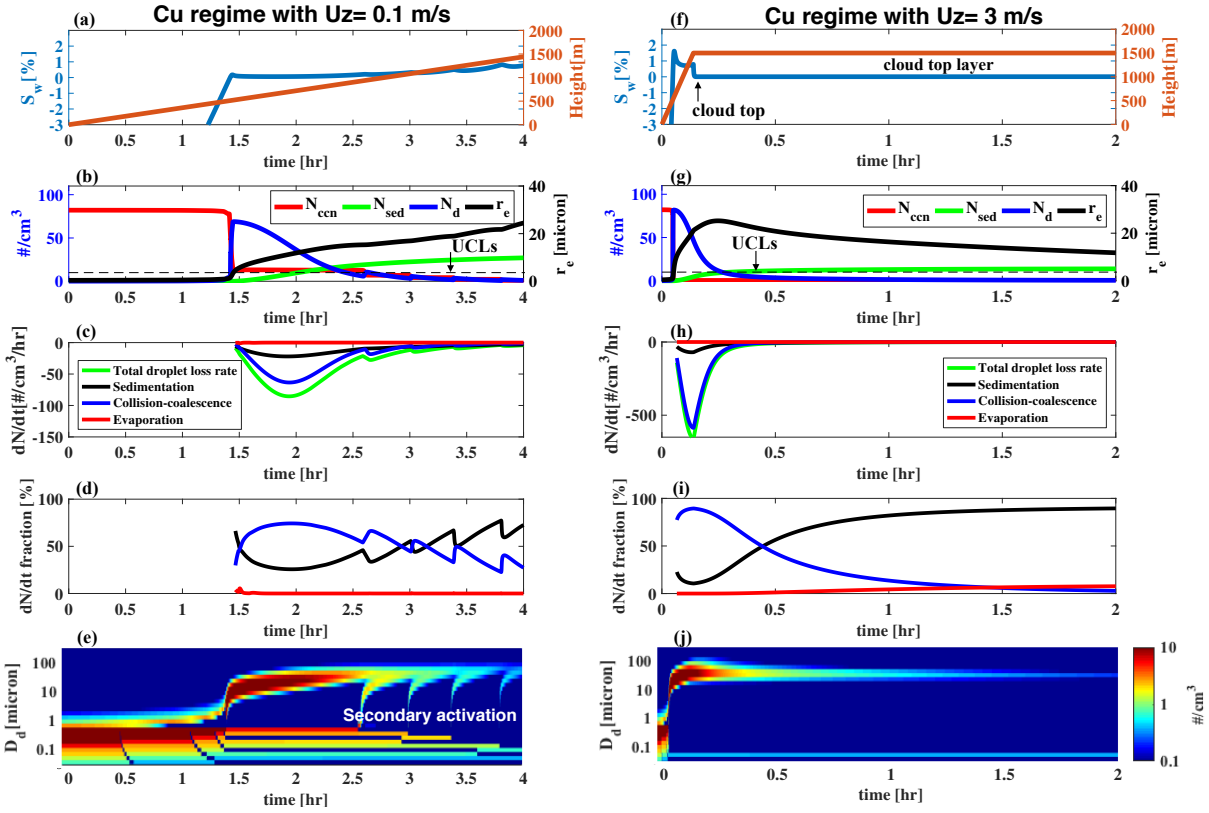

FIG. 7. Cu regime as in figure 5 except for $U_z = 0.1\ ms^{-1}$ and $3\ ms^{-1}$

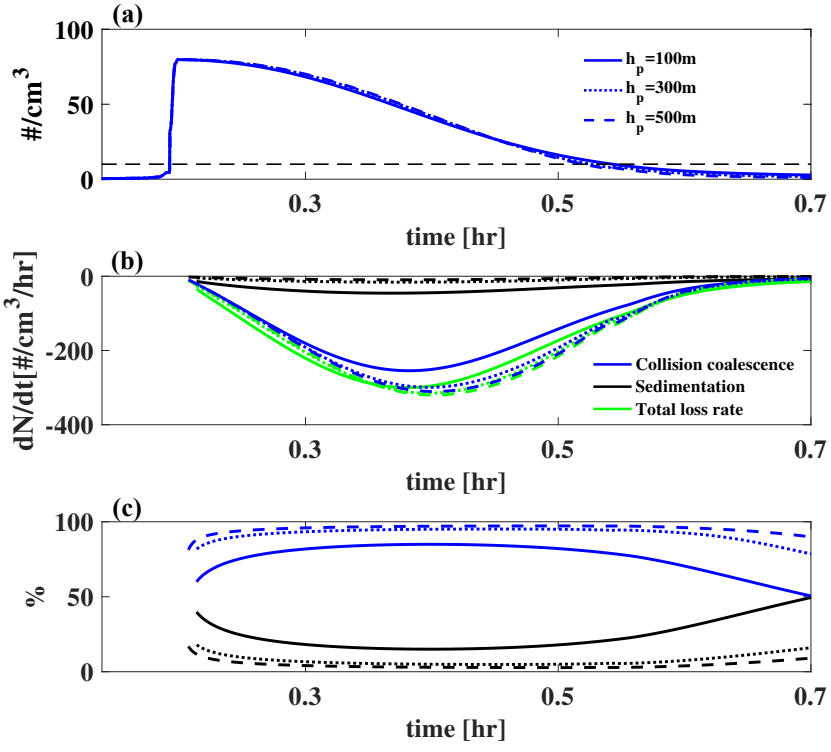

FIG. 8. Sensitivity test to the value of h_p used in the Cu base case ($U_z = 0.75\ ms^{-1}$). solid line: $h_p = 100\ m$; dotted line: $h_p = 300\ m$; dashed line: $h_p = 500\ m$. (a) Temporal evolution of cloud droplet concentration N_d in the parcel; (b) Total droplet loss rate (green), droplet loss rate by collision-coalescence (blue) and sedimentation (black); (c) Fraction of droplet loss rate by sedimentation (black) and collision-coalescence (blue).

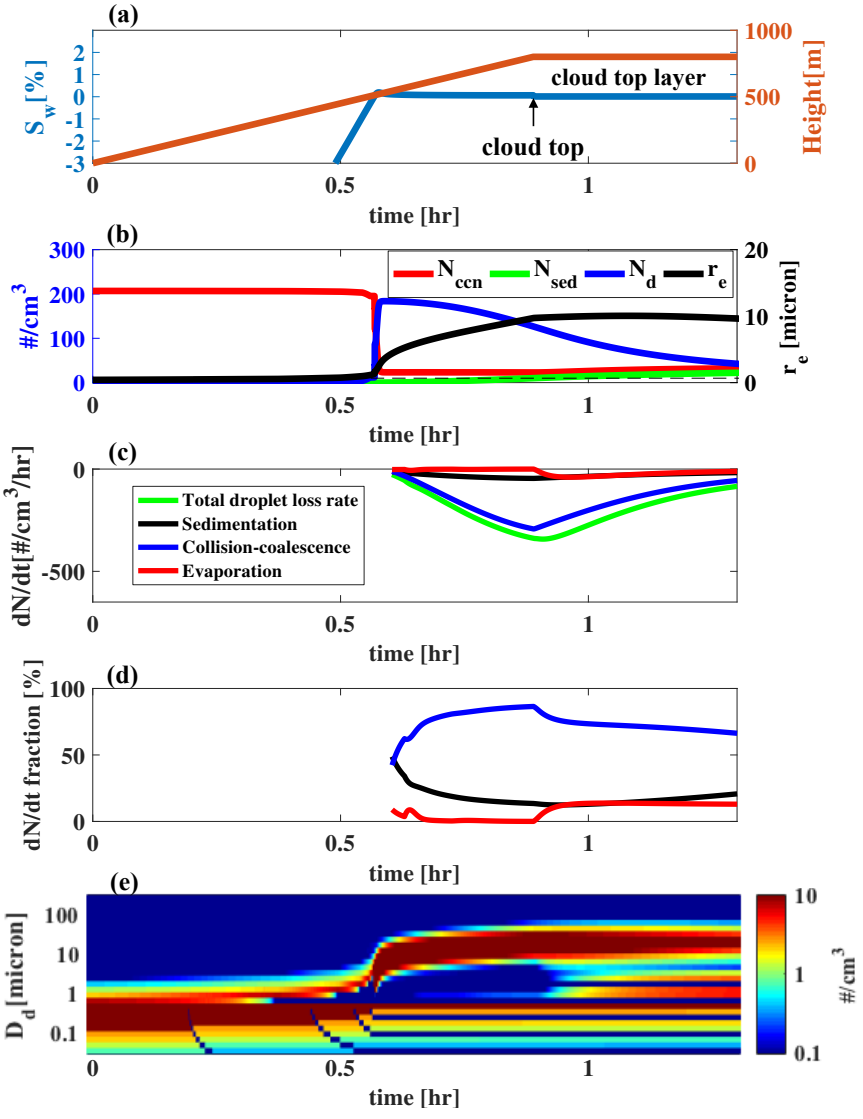

FIG. 9. As figure 5 except for the stratocumulus regime.

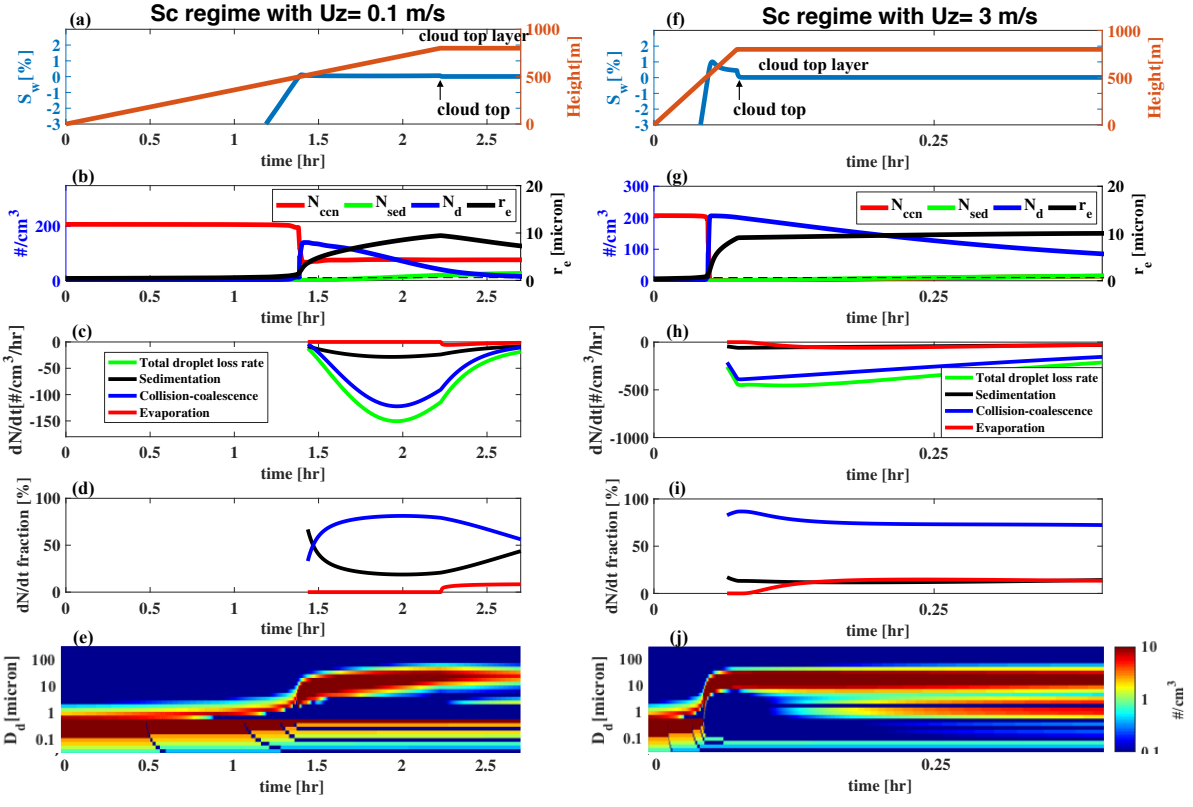

FIG. 10. Sc regime as in figure 8 except for $U_z = 0.1\ ms^{-1}$ and $3\ ms^{-1}$

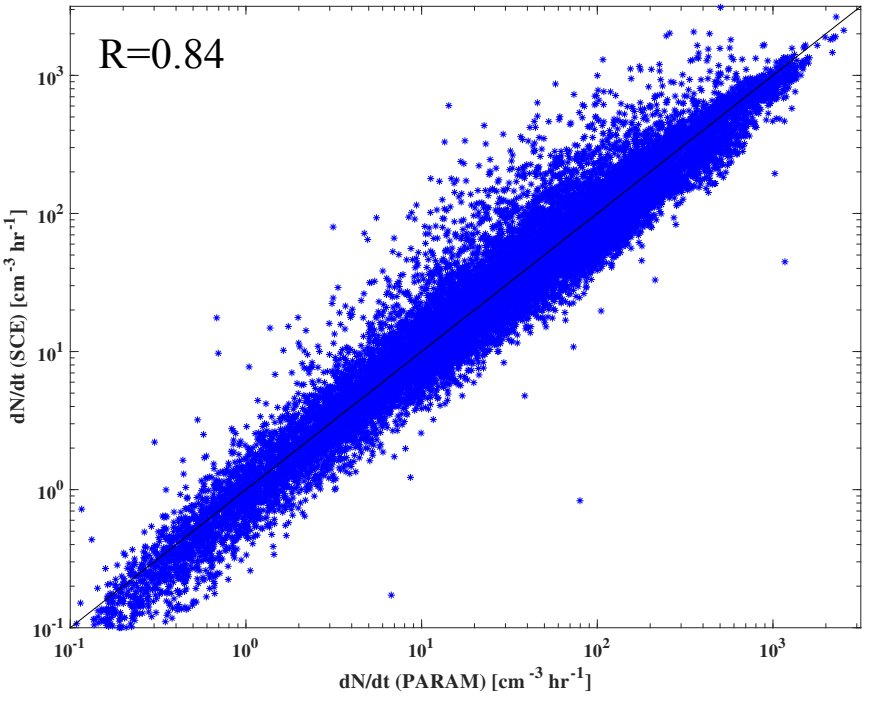

795 FIG. 11. Drop coalescence-scavenging rates estimated by integration of the SCE of Eq. (2) using observed
796 DSDs from CSET against the parameterization given by Eq. (3). The collection kernel used here is described in
797 Sect. 2.

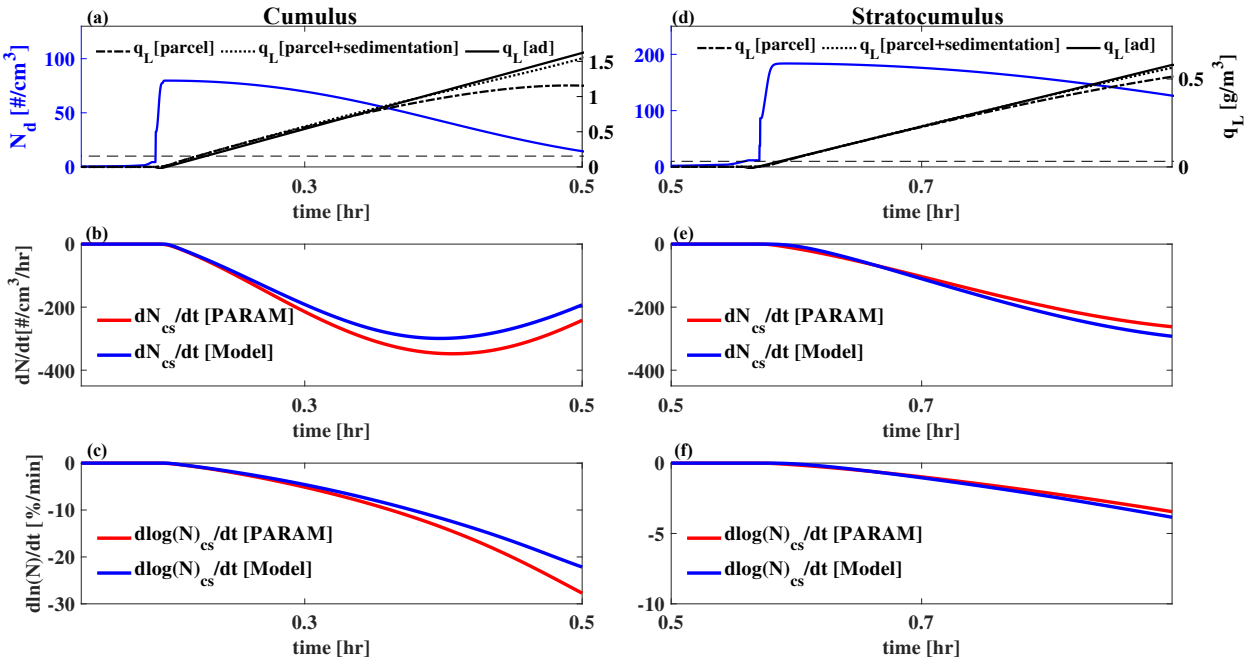

FIG. 12. Comparisons of the droplet coalescence-scavenging rates calculated based on the parameterization and the bin microphysics scheme. (a-c) The cumulus base case; (d-f) the stratocumulus base case. (a,d) The temporal evolution of droplet concentration N_d (blue), liquid water content inside the parcel $q_L[parcel]$ (black dot-dashed), liquid water content inside the parcel + liquid water content lost to sedimentation $q_L[parcel + sedimentation]$ (black dotted), and adiabatic liquid water content $q_L[ad]$ (black solid); (b,e) droplet coalescence-scavenging rates from the parameterization of Eq. (3) and the parcel model; (c,f) fractional droplet coalescence-scavenging rates from the parameterization of Eq. (4) and the parcel model.

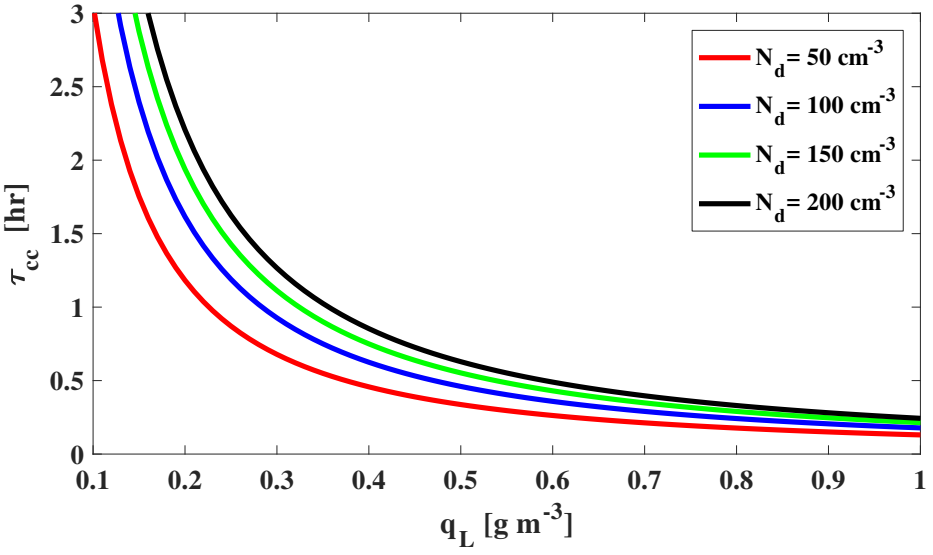

805 FIG. 13. Time scale of droplet loss by collision-coalescence calculated by Eq. (5) as a function of liquid water
806 content q_L.

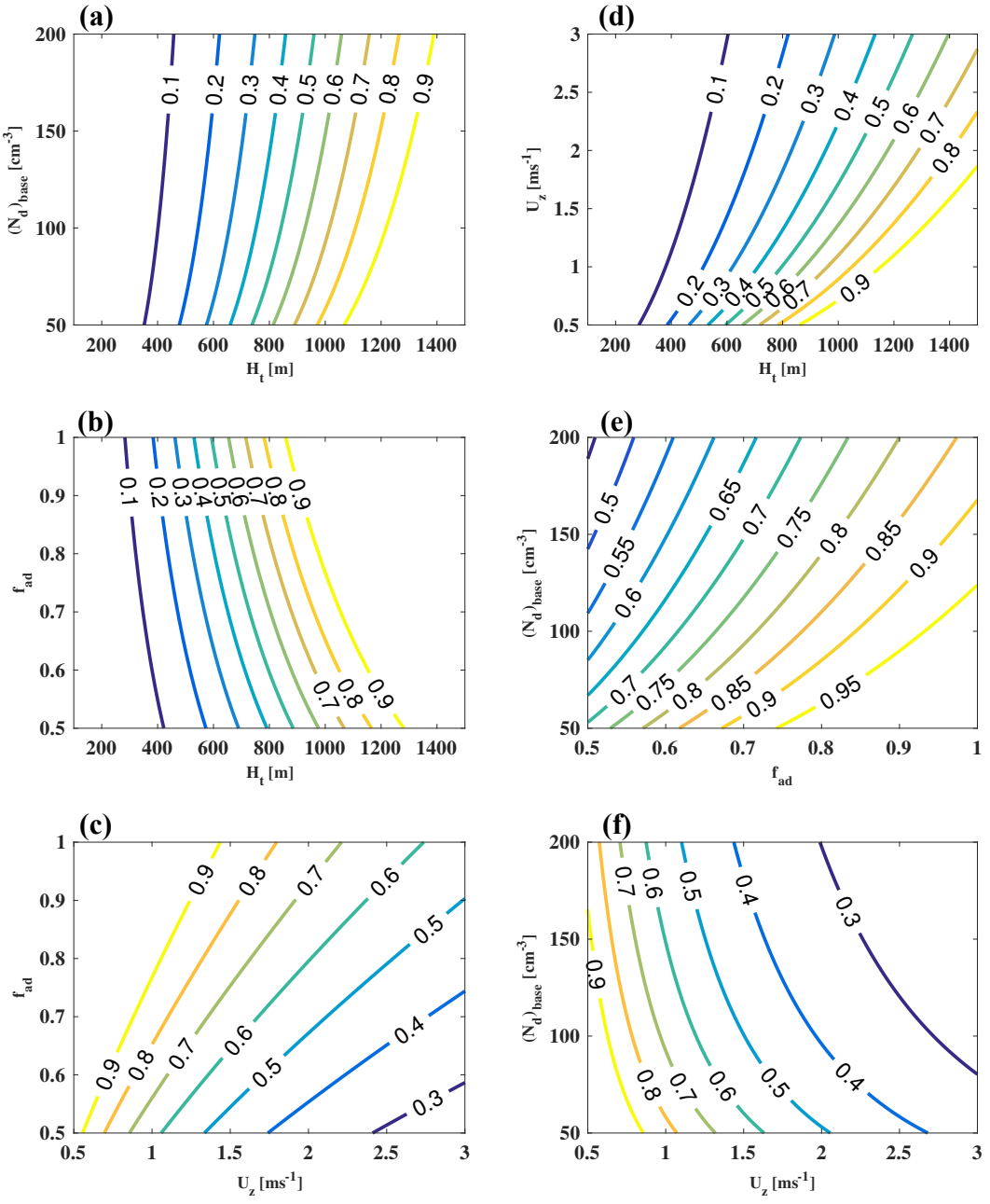

FIG. 14. Contour plots of fractional loss of N_d at the cloud top from the cloud base $f_{top-loss}$ and its dependence on U_z, $(N_d)_{base}$, H_t and f_{ad} calculated using Eq. (10). A reference U_z = 1 ms^{-1}, $(N_d)_{base}$ =75 cm^{-3}, H_t = 1000 m, and f_{ad} = 0.6 are assumed when they are not the variables in the plot (e.g., U_z = 1 ms^{-1} and f_{ad} = 0.6 are assumed in Fig 14-a).

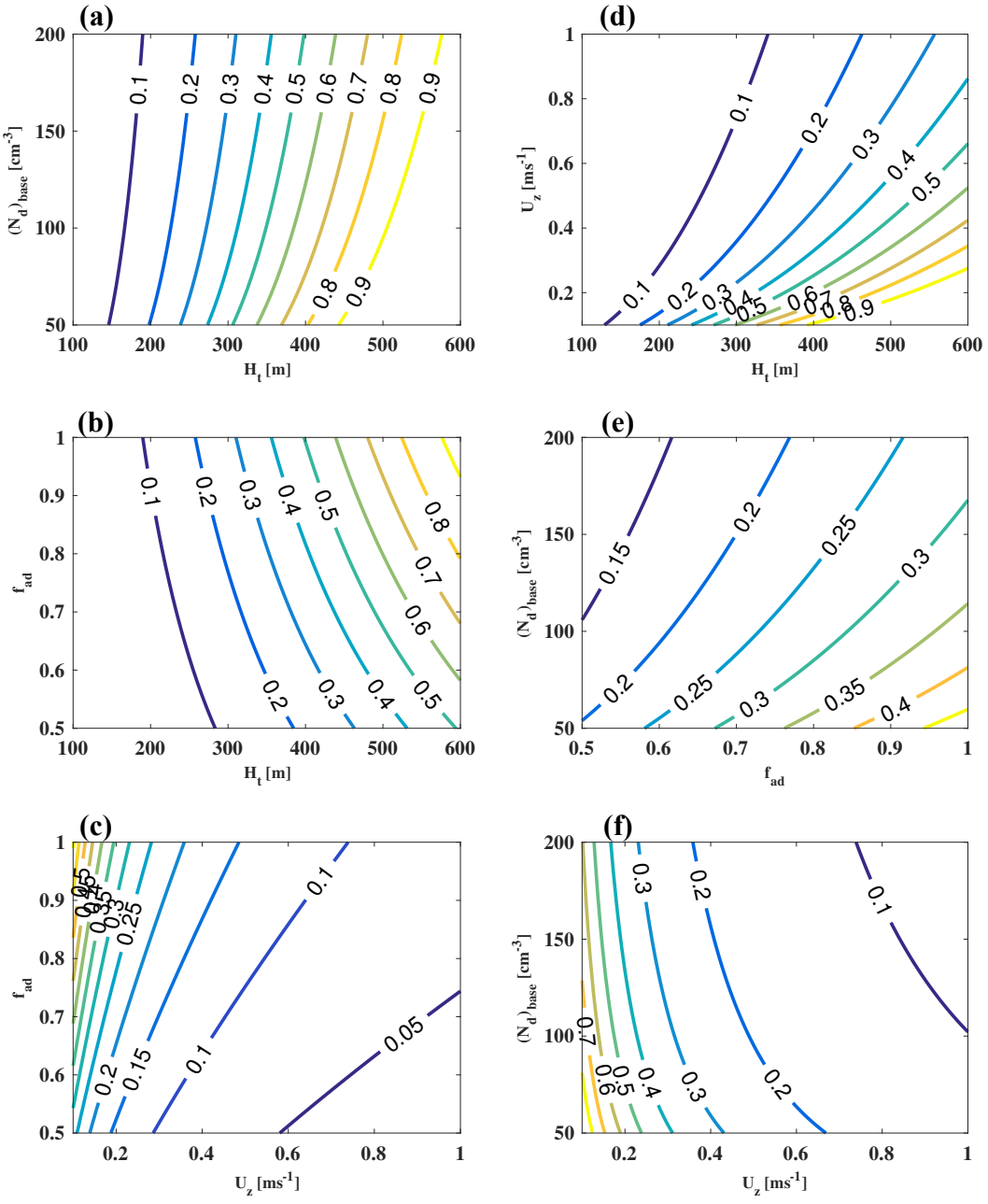

811 FIG. 15. Contour plots of fractional loss of N_d at the cloud top from the cloud base $f_{top-loss}$ and its dependence
812 on U_z, $(N_d)_{base}$, H_t and f_{ad} calculated using Eq. (10). A reference U_z = 0.25 ms^{-1}, $(N_d)_{base}$ =200 cm^{-3}, H_t =
813 300 m, and f_{ad} = 1 are assumed when they are not the variables in the plot (e.g., U_z = 0.25 ms^{-1} and f_{ad} = 1 are
814 assumed in Fig 15-a).